Drug-Drug Interaction Between Oxycodone and Diazepam by a Combined *in silico* Pharmacokinetic and Pharmacodynamic Modeling Approach

Running head: DDI between oxycodone and diazepam

Beihong Ji[1, 2,+], Ying Xue[1, 2,+], Yuanyuan Xu[1, 2], Shuhan Liu[1, 2], Albert H Gough[3], Xiang-Qun Xie[1, 2,*], Junmei Wang[1, 2,*]

[1]Department of Pharmaceutical Sciences and Computational Chemical Genomics Screening Center, School of Pharmacy, The University of Pittsburgh, 3501 Terrace St, Pittsburgh, PA 15261

[2]NIH National Center of Excellence for Computational Drug Abuse Research, The University of Pittsburgh, Pittsburgh, Pennsylvania, 15261, USA.

[3]Computational and Systems Biology, The University of Pittsburgh, Drug Discovery Institute, 800 Murdoch Building, 3420 Forbes Avenue, Pittsburgh, Pennsylvania, 15260, USA.

Beihong Ji: First author, Submitting author, bej22@pitt.edu, School of Pharmacy, University of Pittsburgh

Ying Xue: First author, yix49@pitt.edu, School of Pharmacy, University of Pittsburgh

Yuanyuan Xu: Co-author, yux35@pitt.edu, School of Pharmacy, University of Pittsburgh

Shuhan Liu: Co-author, shl169@pitt.edu, School of Pharmacy, University of Pittsburgh

Albert H Gough: Co-author, gough@pitt.edu, Drug Discovery Institute, University of Pittsburgh

Xiang-Qun Xie: Corresponding author, xix15@pitt.edu, School of Pharmacy, University of Pittsburgh

Junmei Wang: Corresponding author, junmei.wang@pitt.edu, School of Pharmacy, University of Pittsburgh

---

[+]To whom contribute equally to this paper

*To whom correspondence should be addressed

Abstract

Opioids and benzodiazepines have complex drug-drug interactions (DDIs), which serve as an important source of adverse drug effects. In this work, we predicted the DDI between oxycodone (OXY) and diazepam (DZP) in the human body by applying *in silico* pharmacokinetic (PK) and pharmacodynamic (PD) modeling and simulation. First, we studied the PK interaction between OXY and DZP with a Physiologically-based Pharmacokinetic (PBPK) model. Second, we applied molecular modeling techniques including molecular docking, molecular dynamics (MD) simulation, and the molecular mechanics/Poisson Boltzmann surface area (MM-PBSA) free energy method to predict the PD-DDI between these two drugs. The PK interaction between OXY and DZP predicted by the PBPK model was not obvious. No significant interaction was observed between the two drugs at normal doses, though very high doses of DZP demonstrated a non-negligible inhibitory effect on OXY metabolism. On the other hand, molecular modeling study shows DZP has the potential to compete with OXY at the same binding pocket of the active μ-opioid receptor (MOR) and κ-opioid receptor (KOR). MD simulation and MM-PBSA calculation results demonstrated that there is likely a synergetic effect between OXY and DZP binding to opioid receptors, as OXY is likely to target the active MOR while DZP selectively binds to the active KOR. Thus, pharmacokinetics contributes slightly to the DDI between OXY and DZP although an overdose of DZP has been brought to attention. Pharmacodynamics is likely to play a more important role than pharmacokinetics in revealing the mechanism of DDI between OXY and DZP.

Keywords: Oxycodone, Diazepam, Drug-Drug Interaction (DDI), Pharmacokinetic-DDI, Pharmacodynamic-DDI, Physiologically-based Pharmacokinetics (PBPK), Molecular Docking, MD simulations

1. Introduction

Prescription drug abuse and overdose is a growing problem in the United States. The number of deaths per year due to drug overdose increased dramatically. For example, the number increased about 23%, from 38,329 to 47,055 between 2010 and 2014.[1] Although overdose deaths are largely assumed to be the result of excessive opioid administration alone, the percentage of overdose deaths involving at least one specific drug ranged from 67% in 2010 to 78% in 2014, suggesting opioid abusers are often polydrug abusers.[1] Benzodiazepines are also one of the most commonly co-administered drugs and are often prescribed for patients with anxiety disorders, muscle spasms and major depression.[2] From 2004 to 2011, the rate of nonmedical use-related emergency department (ED) visits for benzodiazepines-opioid co-ingestion increased from 11.0 to 34.2 per 100,000 population, while the prevalence of overdose death involving both drugs increased from 0.6 to 1.7 per 100,000 population.[3] Thus, serious risks are associated with the combined use of opioids and benzodiazepines. The Food and Drug Administration of United States added Boxed Warnings to the drug labeling of prescription opioids and benzodiazepines in 2016. It is believed that opioids and benzodiazepines have complex drug-drug interactions (DDIs), which serve as an important and potentially preventable source of adverse drug effects and overdose death. However, there is still much unknown about how these two types of drugs are interacting with each other.[4]

Oxycodone (6-deoxy-7,8-dehydro-14-hydroxy-3-O-methyl-6-oxymorphine), also known as Percocet and Oxycontin, is an opioid drug which acts as an agonist of μ- and κ-opioid receptors.[5, 6] It is often used as a reliever of moderate to severe pain for its effect similar to morphine as well as its high bioavailability (60%) with different formulations, such as oral (most common), intramuscular, intravenous and subcutaneous administration.[7] Oxycodone (OXY) primarily undergoes CYP3A4-mediated N-demethylation to form noroxycodone (NOC) as well as CYP2D6-mediated O-demethylation to form oxymorphone (OM). Both NOC and OM can be further converted into noroxymorphone (NOM).[8] Only a very small amount of oxycodone is metabolized by UDP-glucuronosyltransferases through conjugation.[9] The detailed metabolic scheme of oxycodone is presented in the left panel of **Figure 1**.

Diazepam (DZP) is a long-acting benzodiazepine with its brand name Valium. It is one of the most frequently prescribed benzodiazepine and is widely accepted and used by people for the

treatment of anxiety, muscle spasms, seizures, trouble sleeping, etc.[10] DZP has a calming effect and it can be administered by oral, rectal, intramuscular and intravenous injection. The overdose effects of taking DZP alone are drowsiness, mental confusion and coma. Concurrent use of diazepam and other drugs like alcohol and opiates may be fatal.[11] DZP is mainly metabolized in the liver by cytochrome P450-mediated reactions (**Figure 1**). DZP undergoes CYP3A4 and CYP2C19-mediated bioactivation to yield nordazepam (N-demethylation) (NDZ) and temazepam (3-hydroxylation) (TMZ), respectively. Both metabolites can be further converted to oxazepam.[12] Generally, CYP2C19 contributes majorly to the N-demethylation while CYP3A4 makes its main contribution to the 3-hydroxylation. The bioavailability of DZP is larger than 90% and its plasma protein binding fraction is also very high (approximately 97%).[13] Compared to OXY (3-5 hours), DZP has a much longer half-life (30-56 hours), which is explained by the low hepatic extraction ratio and more extensive tissue distribution of unbound fraction.[13, 14]

Basically, DDIs can be broadly categorized into pharmacokinetic drug-drug interaction (PK-DDI) and pharmacodynamic drug-drug interaction (PD-DDI). For the former, the DDI arises since CYP3A4 is the common major player in metabolism pathways of both OXY and DZP. Indeed, DZP has also been reported as the inhibitor of CYP3A4 in some *in vitro* studies.[15, 16] In our previous work, we have utilized Physiologically-based Pharmacokinetic Modeling (PBPK) models to study DDIs between a series of opioids and benzodiazepines.[17] In this work, we attempt to further study if DZP, which is suggested to be served as an inhibitor of CYP3A4, could alter the pharmacokinetic (PK) profile of OXY *in vivo* when co-administering with DZP by taking more inhibition mechanisms as well as more types of formulations into consideration. Another source of interaction between OXY and DZP comes from pharmacodynamic interactions, i.e. there is a synergic or additive effect for the two drugs acting on their drug targets. It is believed that people may concomitantly take opioids and benzodiazepines to increase the μ agonist effects of opioids. Indeed, some preclinical evidence shows some effects of benzodiazepines like analgesic and anxiolytic are partially mediated by opioidergic mechanisms, even though some contrasting data in terms of the evidence was also reported.[18] Also, it is reported that 72 % of patients who use methadone are also DZP users simultaneously, indicating that DZP can enhance the drug effects of methadone.[19] Hence in this work, we attempt to study if DZP has a positive synergistic effect with OXY by also interacting with the opioid receptors.

Since the DDI studies of the two types of drugs in human subjects are limited, alternative methods for evaluating DDIs at toxic levels in humans are needed. In this work, we attempt to address this problem from both the pharmacokinetic (PK) and pharmacodynamic (PD) perspectives. First, we quantitatively simulated the PK profiles of OXY and DZP by utilizing the PBPK modeling method; we then used hierarchical molecular modeling techniques including molecular docking, molecular dynamics (MD) simulation and molecular mechanics/Poisson Boltzmann surface area-WSAS (MM-PBSA-WSAS) binding free energy calculations to predict the PD interaction between these two drugs. Lastly, we discussed the relative contribution of PK and PD to the DDI between OXY and DZP by analyzing the simulations results at both the normal and overdosed scenarios.

2. Results and Discussion

In this study, we investigated DDI between OXY and DZP by applying *in silico* computational approaches pharmacokinetically and pharmacodynamically. To the best of our knowledge, this is the first time PBPK modeling and molecular modeling techniques have been applied in the DDI exploration. We first established a PBPK model by utilizing SimCYP to predict the DDI between OXY and DZP. As a result, DZP has a limited effect on OXY's metabolism and only a severe high dose of DZP can exert a minor inhibitory effect on OXY. Then we moved on to PD interaction between these two drugs by investigating the pharmacological effect of DZP on the two types of opioid receptors. The molecular modeling study shows that DZP has the potential to compete with OXY at the same binding pocket of the active MOR and KOR. Interestingly, MD simulation and MM-PBSA-WSAS calculation results demonstrated that DZP is able to bind stably with active KOR and has selectivity for KOR. We concluded that pharmacodynamics is likely to contribute mostly to the DDI between OXY and DZP, and there is a synergistic or additive effect when DZP is taken with OXY simultaneously.

2.1 Pharmacokinetic DDI

PBPK modeling has been increasingly used for the prediction of DDIs recently, especially for the prediction of CYP-mediated DDIs.[20] PBPK modeling utilizes *in vitro* drug data (e.g. intrinsic clearance and bioavailability) describing a drug's ADME properties and utilizes system data depicting the physiological properties of human subjects in a population, to explore the *in vivo* pharmacokinetics of drugs and DDIs scenarios. The PBPK approach has been valued by the US

Food and Drug Administration (FDA) and the European Medicines Agency (EMA) through the guidelines for DDIs in 2012 and 2013.[21] Moreover, PBPK modeling currently receives high attention in the drug development and drug discovery process. A full PBPK model is probably the most complicated PK model existing currently, which consists of different organs in the human body linked by blood circulation. A PBPK model is different from the empirical PK model and has multiple compartments being included. As a result, DDI modeling and simulation based on a PBPK model are closer to the real situation than that of an empirical PK model. In this study, the transporter-mediated DDI was not considered in our model because there is limited clinical evidence that shows transporters, such as those found in the blood-brain-barrier (BBB), cause significant interactions between the two types of drugs. We also did not include the inhibitory abilities of metabolites given the fact that the concentration of metabolites of DZP is only approximately one-tenth of the concentration of the parent drug. Since both drugs go through the metabolic pathway by CYP3A4, and the docking results showed that DZP had better binding affinity than OXY when binding to CYP3A4, we mainly studied the effect of DZP on OXY.

2.1.1 Validation of PBPK models for OXY and DZP

First, we validated the PBPK models of OXY and DZP by creating models and generating PK profiles for them individually. We collected experimental data of plasma Concentration ~ Time (CT) curves for these two drugs from the literature, and the data were used to verify our models. The ADME profiles for OXY and DZP as well as their metabolites were predicted by using SimCYP software and are listed in **Table S1**. Some of the PK parameters were collected from the literature, while others came from SimCYP internal databases, still others were predicted by SimCYP calculators. Then we created an oral (PO) model for 30 mg OXY, an intravenous (IV) model for 0.1 mg/kg DZP and a PO model for 10 mg DZP according to the recommended dosages of the two drugs. In the PO OXY model, the absorption was described as a first order process, while in the PO DZP model, the procedure was described by the ADAM absorption model implemented in the SimCYP software. For the IV DZP model, DZP was modeled to enter the systemic circulation by venous blood vessels. Experimental PK data obtained from the literature which included area under the curve (AUC), maximal concentration (C_{max}) and time of maximal concentration observed (T_{max}) were used to verify our PBPK models. Last, we compared how different formulations affected how DZP interacted with OXY.

The observed and predicted PK data are listed in **Table 1.** The C_{max} and T_{max} of DZP are missing due to the limitation of existing experimental studies. The CT curves for OXY and DZP are depicted in **Figure 2**. From the **Table 1** and **Figure 2,** we can see that all the predicted AUC, C_{max} and T_{max} of OXY and DZP were within the ranges of their observed data (within the standard deviations (SD)). All the CT curves ranged from 0 to 24 hours except for PO DZP, for which our predicted CT data of PO DZP was only limited to 12 hours for the sake of comparison.

2.1.2 DDI simulation following competitive inhibition mechanism

Since the interaction between two different substrates with the same enzyme is commonly considered as competitive inhibition,[22] we first hypothesized that DZP is a competitive inhibitor of CYP3A4 and can inhibit the metabolism of OXY which is predominately metabolized by CYP3A4. Hence in our PBPK models, OXY served as the substrate while DZP served as the inhibitor. We estimated the inhibitory constant, K_i value, by using the Glide docking score, because currently there is no available experimental K_i value for the two drugs binding to the cytochromes P450 enzymes. The K_i parameter of DZP was calculated by **Eq. 2** and other input parameters are listed in **Table S1**. DDI models for OXY and PO/IV DZP were built using the calculated K_i in addition to the other PK parameters (**Table S2**). To better compare the DDI effect between OXY and DZP, we adjusted the dosage of DZP from normal to overdose. The AUC of the substrate was then compared between substrate and substrate-inhibitor profiles to investigate the DDI between these two drugs. The simulated concentration profiles of 30 mg OXY co-administered with different doses of PO DZP are shown in **Figure 3**. The predicted AUC Ratios and C_{max} Ratios of the DDI profiles with and without the presence of DZP are shown in **Table 2**.

As shown in **Figure 3**, the OXY concentration raise can only be remarkably observed when the dosage of PO DZP reaches to 1000 mg. The plasma concentration of OXY increases as the administrated dosage of PO DZP increases, but the difference is not obvious for low doses of PO DZP. Correspondingly, both of the AUC_{24h} (the drug exposure from time zero to 24 hours) ratio and C_{max} ratio are 1.01 with the co-treatment of 30 mg PO OXY and10 mg of PO DZP. The AUC ratio increases by 4.0% when the dose of PO DZP increases to 10 times of the normal dose. Only when the dose of PO DZP was increased to 1000 mg can the simulated interaction between OXY and PO DZP result in a growth of AUC of OXY by 1.20 folds, which is a commonly used threshold to determine whether two drugs have a DDI or not. The C_{max} of OXY increased to 1.12 folds when the dosage of PO DZP was 1000 mg. Accordingly, 1000 mg IV DZP exhibited a similar but weaker

PK effect compared to the simulation result of PO formulation. The comparison of AUC Ratio for OXY with different formulations of DZP is shown in **Figure 4**. The AUC ratio of OXY with PO DZP is a little bit higher than with the same dosage of IV DZP as suggested by **Figure 4**. As a result, the inhibitory ability of oral administration of DZP is slightly stronger than DZP with IV administration. The reason for causing this difference might be the relatively smoother change of PO DZP concentration since PO drug does not directly go into blood circulation while IV formulation does.

According to the report in 2005,[23] the toxic concentration of OXY is 690 ng/mL, which is much higher than the C_{max} of the 30 mg OXY when taken together with 1000 mg DZP. Even though there is a report about taking DZP over 1000 mg,[24] the dosage of 1000 mg still greatly exceeded the normal dose and lacked clinical meaning. According to the literature, when the plasma concentration of the DZP was as high as 4792 ng/mL, patients were minimally sedated and were discharged within 24 h.[25] To mimic this realistic case, in our model, we set the dosage of PO DZP as 200 mg and its maximal concentration was predicted as 4500 ng/mL. Then we used a full PBPK model to simulate DDI for co-administration of 30 mg OXY and 200 mg DZP. It was found that there was almost no PK interaction between these two drugs (AUC ratio = 1.08, C_{max} ratio = 1.06).

Similarly, we also investigated how PK profiles of DZP were affected by OXY. After changing the roles of OXY and DZP, the results of DDI between the two drugs were consistent with the previous findings. The AUC ratio of 10 mg DZP with the administration of 30 mg OXY is 1.01; even though the dosage of OXY was increased to 500 mg, the AUC ratio only changed slightly to 1.07.

We also studied how the different multiple-dosage regimens and long period of drug administration affect the PK-DDI between OXY and DZP. Our simulation result suggests that there is no or little PK-DDI between OXY and DZP under those circumstances.

Given the limitations of docking scoring function, such as the lack of structural flexibility of target protein, there is possibility that the estimated K_i, which calculated from the docking score, is not accurate enough. Hence to minimize the potential source of error, the additional sensitivity analysis for K_i was also conducted for the DDI model between OXY and PO DZP by changing the K_i value from 0.165 μM to 165 μM in order to find out the impact of K_i value on the simulation results. A surface plot which depicts the change of the AUC ratio of OXY with the change of the

K_i value of the dosage of DZP was created (**Figure S4**). When concurrently taking 30 mg OXY and different dosages of DZP (from 10 mg to 1000 mg) with the K_i ranging from 0.165 μM - 165 μM, the corresponding AUC ratio of DDI moved from 1.000 to 1.375, indicating the error of K_i does not have a significant influence on the prediction of DDI between these two drugs. Even though a relatively low K_i and a very high dosage of DZP (1000 mg) are considered, the exposure of OXY still shows no significant growth with the presence of DZP. The results imply that the PK interaction between OXY and DZP is very weak and has little clinical meaning,

2.1.3 DDI simulation following mixed-type inhibition mechanism

Although it is believed that competitive inhibition is the inhibition type that most commonly happens between two substrates for the same enzyme, the interaction between CYP3A4 substrates can always become more complicated, considering the inactivation of the enzyme in the realistic situation. Therefore, in this study, we combined the competitive inhibition with the mechanism-based inhibition in modeling the DDI of OXY and PO DZP. The concentration of the mechanism-based inhibitor associated with half-maximal inactivation rate (K_{app}) and the inactivation rate of the enzyme (K_{inact}) is listed in **Table S1**. The detailed mechanisms of competitive and mechanism-based inhibitions have been described in the Methods Section. The comparison of the AUC ratio of OXY with different dosages of PO DZP under the competitive inhibition and mixed-type inhibition is displayed in **Figure 4**. In addition, the detailed AUC ratio of DDI profiles based on mixed-type inhibition is listed in **Table 3**. According to the results, the AUC and C_{max} Ratios predicted by using the mixed-type inhibition mechanism are slightly higher than the competitive inhibition as discussed in **2.1.2**. To conclude, the inhibitory effect of DZP is slightly stronger when applying a mixed-type inhibition mechanism to the DDI model of OXY and DZP, especially when DZP is overdosed. For example, the AUC ratio in the mixed-type inhibition model is 8.3% higher than the AUC ratio predicted by the simple competitive inhibition model.

2.2 Pharmacodynamic DDI

To better investigate the PD DDI between OXY and DZP, we performed molecular docking and MD simulation sequentially for OXY and DZP as well as other typical opioid modulators (4VO, BF0, CVV, JDC) targeting to both the MOR and KOR.

2.2.1 Molecular docking

To predict the binding affinity between ligands and receptors as well as the features of the binding sites of models, docking analysis was performed on several ligands, including opioid agonists (OXY, 4VO and CVV), opioid antagonists (BF0 and JDC), and DZP towards MOR and KOR. The docking results of opioids and DZP are summarized in **Table 4**. The docking performance of a ligand is considered to be better when the docking score is lower. As shown in **Table 4**, the docking results of opioids are reasonable, as native co-crystallized ligands all show better performance when binding to their own crystal receptors. In **Table 4**, among four co-crystallized ligands, 4VO and CVV are the two agonists, while BF0 and JDC are the two antagonists. For an agonist, either 4VO or CVV, its docking score to the active receptor is always better than that of binding to the inactive receptor. While for an antagonist, the docking score binding to an inactive receptor is better than that of binding to an active one. Those docking results are very reasonable.

As to OXY and DZP, both have comparable docking scores to either active/inactive MOR and KOR. The docking scores with active opioid receptors are slightly better than the corresponding inactive opioid receptors, suggesting OXY and DZP are more likely as agonists. However, the docking result of OXY is unexpected since it exhibits a worse docking score than that of JDC, an antagonist of KOR. Overall, the docking results of DZP are acceptable: it has a better docking score than OXY when binding to active MOR and a similar docking score to OXY when it binds to inactive KOR. From the docking results, we can preliminarily infer that DZP might be able to compete with OXY at the same binding pockets of the active MOR and KOR. Unfortunately, although the docking method is efficient, it is still not accurate enough since its performance only reflects the static binding situation and mainly depends on how well the binding pocket of the native ligand resembles the ones for OXY and DZP.

2.2.2 Molecular dynamics simulation

Unlike the docking method, MD simulations can reflect the dynamics of interaction between ligand and protein and can better mimic the realistic situation. To investigate the dynamics of ligand binding, MD simulations were also performed for these two systems: active/inactive MOR and active/inactive KOR in complex with opioids and DZP. The starting conformations of MOR/KOR in complex with ligands were selected from the best flexible docking poses. We adopted the statistic parameter, root-mean-square deviation (RMSD) to measure the fluctuation of a ligand and its receptor against the starting conformation of the simulation, which is either the

crystal structure if the ligand is the native ligand of the crystal structure or the best docking pose otherwise. The RMSD values as well as the fluctuation of RMSD curves were applied to measure the dynamic stability of a ligand binding. We calculated four types of RMSDs for different subsets of atoms, including the main chain atoms of the receptor (black curve, Type 1); the main chain atoms of the seven transmembrane domains (red curve, Type 2); the ligand with the consideration of all its movement and conformational changes (labeled as "Non-Fitting Ligand," orange curve, Type 3); and the ligand after aligned to its initial conformation (labeled as "Fitting Ligand," purple curve, Type 4). To calculate the Type 3 RMSDs, we first performed the least-square fitting for the 7TM main chain atoms, then the resulting translation-rotation matrix was applied to the ligand and the RMSDs were calculated directly. The "Non-Fitting ligand" RMSDs not only measure the conformational changes of the ligand during the MD simulations, but also its translation and rotation movements inside the binding pocket. The time courses of those RMSDs are shown in **Figure 5**. The representative conformations aligned to the corresponding initial structures are shown in **Figure 6**.

For the MOR system, overall, the Type 1 and Type 2 RMSDs are lower than 3 Å, except for OXY, whose RMSDs are slightly larger than 3 Å when binding to the active MOR (**Figures 5A-H**). As expected, all four types of RMSDs are very small and stable for 4VO binding to the active MOR, and the Type 3 RMSDs are much larger when 4VO is bound to the inactive MOR. Similarly, the observations for BF0, an antagonist of MOR are also reasonable (**Figures 5B, 5F**). For OXY, the two ligand RMSDs binding to active MOR are larger than when binding to inactive MOR. In contrast, DZP is much more stable when binding to the active MOR.

As for the KOR system, the Type 1 and 2 RMSDs are all lower than 3 Å and relatively stable. For CVV, the native ligand of the active KOR, the RMSD curves when binding to active KOR are lower and more stable than when binding to the inactive KOR. However, the corresponding RMSD curves are similar for JDC, an antagonist, when binding to either the active or inactive KOR. As to OXY, the corresponding RMSD curves are also similar when binding to active or inactive KOR. Unlike OXY, DZP demonstrates higher stability when binding to the active KOR than to inactive KOR. Particularly, the Type 3 RMSDs of DZP are larger than 5.0 Å when binding to inactive KOR, suggesting the docking-predicted pose may not be energetically favorable. This finding could be partially validated by an *in vitro* study in 2001, which explored the potential interactions of benzodiazepines with cloned human opioid receptor subtypes and

implied that three other benzodiazepines- midazolam, chlordiazepoxide, and diazepam- were agonists for KOR.[26] More interestingly, as suggested by the RMSD curves of DZP bound to the inactive KOR, both the receptor and the ligand underwent a larger fluctuation during the MD simulation and the ligand significantly drifted away from the initial docking binding pose (**Figure 5P**). In contrast, the RMSD curves are more stable and RMSD values are much smaller for DZP bound to the active KOR, indicating a strong selectivity of DZP towards KOR.

2.2.3 MM-PBSA-WSAS calculations

To further understand the PD-DDI between OXY and DZP, we conducted MM-PBSA-WSAS free binding energy calculations. The calculated binding free energies and individual energy terms for MOR and KOR systems are shown in **Table 5**. Of note, the absolute binding affinities may be overestimated or underestimated by the MM-PBSA-WSAS method, and one should focus on the relative binding free energies. Encouragingly, the results of binding free energy calculations were consistent with the results of stability analysis on the MD trajectories, indicating the reliability of our binding free energy method. For the active MOR, DZP (-1.33$\pm$0.05 kcal/mol) had a binding energy comparable to that of OXY (-1.19$\pm$0.11 kcal/mol); while for inactive MOR, OXY has apparently more potent binding affinity (-5.40 kcal/mol) than DZP (1.07 kcal/mol). DZP had a much more potent binding than OXY to the active KOR, while OXY had a much more potent binding than DZP to the inactive KOR. Taken together, DZP is likely to selectively bind to active KOR as an agonist since its binding free energy is much lower ($\Delta\Delta G_{bind}$ = -5.27 kcal/mol) than that of binding to the inactive KOR. Encouragingly, this result is consistent with the experimental findings by Cox and Collins,[26] who pointed out that diazepam directly displaced displaced [(3)H]-diprenorphine binding from κ and δ-opioid receptors, but not the μ receptor.

Although OXY has the best binding affinity to the inactive MOR, it is regarded as an agonist of opioid receptors.[27] Comparing the binding affinities of OXY to the active opioid receptors, apparently, it can bind to the active MOR with a better binding affinity (**Table 5**); this observation agrees with the known fact that OXY is a μ-opioid receptor agonist.[28, 29] Overall, our MM-PBSA-WSAS free energy results are reasonable. Irrespective of the kinetics of OXY and DZP binding to MOR or KOR, there is very likely a synergic effect when DZP is co-administered with OXY, as it binds to active KOR while OXY binds to active MOR. The detailed ligand-protein interactions are illustrated in **Figure 7**. It is shown that OXY forms one hydrogen bond with

histidine (HIS)-297 in active MOR, and two hydrogen bonds with lysine (LYS)-227 and aspartic acid (ASP)-138 in active KOR. On the other hand, DZP forms a Pi-Pi stacking interaction with tryptophan (TRP)-287 using its phenyl function group in active KOR system. However, no favorable interaction was identified between DZP and active MOR. In summary, there is a pharmacodynamic DDI between OXY and DZP.

2.3 Limitation and future work

Even though the study has been well designed, there are still some limitations. For the PK-DDI study, first, we relied on molecular docking to predict the kinetic parameters for the mechanistic model. The docking method may not be an accurate tool to estimate binding affinities. More advanced molecular modeling techniques on endpoint free energy calculations[30-32] will be applied to this project in the future. Second, clinical data for these two drugs are limited and *in vivo* experiments are needed in the future. Moreover, a metabolite of OXY, oxymorphone, an active metabolite which can produce a similar effect as OXY, was not included in our PBPK model.[13]

For the PD-DDI study, we performed MM-PBSA-WSAS analysis to calculate binding free energies. Although this endpoint method has gained its popularity recently,[31-34] the performance of this method is overall inferior to the alchemical free energy-based methods, like free energy perturbation,[35] thermodynamic integration (TI).[36] In the future, we will apply thermodynamic integration method to study PD-DDIs between opioids and benzodiazepines. Last, as most studies in the field of drug design, the kinetics of OXY and DZP binding to the opioid receptors was not taken into account to explore their synergic effect.

Conclusion

In our study, we developed the PBPK model and conducted molecular modeling to study DDI between OXY and DZP pharmacokinetically and pharmacodynamically. Overall, there is no PK-DDI between the normal doses of OXY and DZP, but DDI can be expected to occur when DZP is highly overdosed. The inhibitory effect of oral administration of DZP on OXY is slightly stronger than that of IV administration. From the PBPK model, we predicted that the PK only contributes marginally to the DDI between the two drugs. In the PD-DDI study, we mainly explored the effect of DZP on two types of opioid receptors in both the active and inactive forms and found the PD-DDI is the major factor that causes the interaction between OXY and DZP.

Based on the results of molecular modeling study, DZP may exert a synergistic or additive effect on the opioid receptors when it is co-administered with OXY. In a conclusion, the DDI between OXY and DZP is mainly caused by pharmacodynamic interaction, but pharmacokinetic interaction also makes a contribution when one or both drugs are severely overdosed.

4. Methods and Materials

4.1 Pharmacokinetic DDI

For PK-DDI study, we applied PBPK modeling to investigate the possible DDI between OXY and DZP using the SimCYP software (Version 17 Release 1, Sheffield, UK). First of all, the whole body PBPK models for both OXY and DZP were separately constructed and the models were validated by using the experimental data. Then, we developed a PBPK-based DDI model by including DZP as an inhibitor in the PBPK model of OXY. DDI simulations were performed by using a virtual healthy population of 100 subjects with the defaults of system data. Drug data including the normal dose of OXY and DZP came from the literature or were predicted by SimCYP if not available. All the system-related parameters came from the SimCYP internal database. The details of all the parameters above are listed in the Supplemental Material.

4.1.1 Inhibitory constant calculation

Since there is no experimental data of the K_i (inhibitory constant) value of OXY and DZP binding to their metabolic enzymes (such as CYP3A4), we performed molecular docking simulations to estimate the K_i values. The selected docking poses not only have the similar binding modes as that of the co-crystallized ligand, but also have the best docking scores. Then the K_i values for a typical enzyme-catalyzed reaction (**Eq. 1**) were calculated by **Eqs. 2-3**.[37]

$$S \underset{k_r}{\overset{k_f}{\leftrightarrow}} ES \xrightarrow{K_{cat}} E + P \quad \textbf{(1)}$$

$$\Delta G^0 = -RTlnK_{eq} = -RTln\frac{k_f}{k_r} \quad \textbf{(2)}$$

$$K_i = \frac{[E][I]}{[EI]} = \frac{k_r}{k_f} \quad \textbf{(3)}$$

Where k_f is the forward reaction rate constant of E+S, k_r is the reverse reaction constant describing rate of falling apart to E+S from ES (enzyme-substrate complex), and K_{cat} is the rate constant of

the irreversible reaction of generating product P from ES. $K_{eq} = k_f / k_r$, is the equilibrium constant for the reversible reaction of forming ES. ΔG^0, the binding free energy, can be estimated using the Glide docking score (kcal/mol) as Glide docking scoring function was trained to reproduce experimental binding free energies.[38]

4.1.2 PBPK modeling.

A PBPK model consists of multiple compartments which represent different physiological organs of the human body. The blood circulation system links all of the compartments. Similar full PBPK models were built for both drugs, and the major difference between the models comes from the absorption processes. The absorption of OXY is described by the first-order absorption model, while the Advanced Dissolution, Absorption and Metabolism (ADAM) model was applied to describe the absorption process of diazepam. The ADAM model implemented in SimCYP considers the complicated process of drug absorption and interplays with the underlying physiological characteristics of the gastrointestinal (GI) tract.[39, 40] The generic full PBPK model and ADAM model are shown in **Figure S1**.

The SimCYP Simulator was used in the development of PBPK models. The Simulator, which can link the *in vitro* experimental data to the *in vivo* absorption, distribution, metabolism and excretion (ADME) and PK/PD outcomes, is able to facilitate us to develop a dosing strategy and to inform product labeling. We chose the healthy volunteer population in the SimCYP database to predict the PK profiles of drugs. All of the PK parameters for the two drugs are summarized in **Table S1.**[41-43 7, 8, 12, 13, 15, 44-50] The docking poses for OXY and DZP are shown in **Figure S2**. The docking scores and calculated K_i are listed in **Table S2**. We also conducted sensitivity analysis to investigate the impact of K_i values towards the DDI effect, utilizing the built-in sensitivity analysis function in SimCYP.

Besides competitive inhibition, mixed-type inhibition which includes both the competitive and mechanism-based inhibitions, was applied to predict the DDI between two drugs. Mechanism-based inhibition occurs when a drug binds to the CYP enzyme fully or partially irreversible (e.g. forming covalent bonds), which inactivates the CYP enzyme and changes PK parameters, such as concentration of inactivator required for the half-maximal inactivation and inactivation rate of enzyme (k_{inact}).[51] The schematic diagram of mechanism-based inhibition is exhibited by **Eq. 4**.[37] The k_{inact} and k_{app} were evaluated by fitting and extrapolating **Eq. 5**[37, 52] which describes the

relationship between the observed inactivation rate constants (K_{obs}) and the concentration of the test inhibitor ($[I]$).

$$\begin{array}{ccccc} E+S & \overset{k_f}{\leftrightarrow} & ES & \xrightarrow{k_{cat}} & E+P \\ & k_r & \downarrow k_{inact} & & \\ & & Inactivated\ Enzyme & & \end{array} \quad \textbf{(4)}$$

$$K_{obs} = \frac{K_{inact} \times [I]}{K_{app} + [I]} \quad \textbf{(5)}$$

4.2 Pharmacodynamic DDI

For PD-DDI study, to determine if OXY and DZP have a synergistic or additive effect on the opioid receptor, we decided to investigate how strong DZP binds to μ- and κ-opioid receptors by utilizing molecular modeling techniques, including molecular docking and MD simulation and MM-PBSA-WSAS energy calculation. Agonist-bound μ- and κ-opioid receptors were obtained from the Protein Data Bank (http://www.rcsb.org). Molecular docking, MD simulation and MM-PBSA-WSAS calculations were performed sequentially as described below.

4.2.1 Molecular docking

Molecular docking was performed using the Glide module of the Schrodinger suite of software (Maestro, version 11.2) for the aforementioned receptors: active μ-opioid receptor (MOR) (PDB entry: 5C1M, co-crystallized agonist 4VO (BU72)) and inactive MOR (PDB entry: 4DKL, co-crystallized antagonist BF0 (β-funaltrexamine)), active κ-opioid receptor (KOR) (PDB entry: 6B73, co-crystallized agonist CVV (MP1104)) and inactive KOR (PDB entry: 4DJH, co-crystallized antagonist JDC (JDTic)). For each receptor, the "Protein Preparation Wizard" was applied to prepare the receptor structure for the Glide docking including adding hydrogens, creating disulfide bonds, conducting restraint minimization, etc. Glide grid was then generated with the default setting, such as, the van der Waals radius scaling factor is 1.0 and partial charge cutoff is 0.25. The grid site was automatically set to the central location of workspace ligand and its size was manually adjusted to match the size of co-crystallized ligand without any constraints or rotatable groups. In total, six ligands were selected for the docking studies: two co-crystallized ligands (4VO and BF0) of μ-opioid receptors (5C1M and 4DKL), two co-crystallized ligands (CVV and JDC) of κ-opioid receptors (6B73 and 4DJH), OXY and DZP. The 2D and 3D structures of the above six ligands are shown in **Figure S3**. To explore the pharmacological effects of

metabolites, OM, TMZ and NDZ were also docked to opioid receptors (See 2.2.1 Molecular docking). Flexible ligand docking was finally performed with the default setting (the van der Waals radius scaling factor is 0.80, partial charge cutoff is 0.15 for ligands, no constraints, etc.) except that the "reward intramolecular hydrogen bonds" was turned on and the maximal poses per ligand was set to 10. In most situations, the best docking poses ranked by the Glide "Standard Precision" docking scoring function, are selected for the subsequent modeling studies. Sometimes, other top docking poses are selected if they can much better overlap with the conformation of co-crystallized ligands.

4.2.2 Molecular dynamics simulation

The basic conformations of the membrane for the opioid receptor complex were built using CHARMM-GUI[53] by adding 240 POPC (1-palmitoyl-2-oleoyl-sn-glycero-3-phosphocholine) lipid molecules. The complexes were immersed in a cuboid box with TIP3P water molecules[54] in all three dimensions. A set of Na^+ and Cl^- ions were added to make a 0.15 M concentration of NaCl and to neutralize the whole system. In molecular mechanics (MM) minimizations and MD simulations, FF14SB[55] and the General Amber force field (GAFF)[56] were applied to describe the protein and ligand molecules, respectively. The atomic partial charges of ligands were derived by restrained electrostatic potential (RESP)[57] to fit the HF/6-31G* electrostatic potentials generated using the Gaussian 16 software package.[58] All the residue topologies of ligands were generated using the Antechamber module.[59]

MD simulations were conducted using the PMEMD.mpi and PMEMD.cuda modules in the AMBER 16 package.[60-62] At first, to dedicatedly remove possible steric clashes in the systems, five constrained energy minimizations were performed by applying a gradually reduced harmonic restraint force constants, from 20 to 10, 5, 1 and 0 kcal/mol/ $Å^2$, to both the main chain residues of the protein and the ligand. Water and ions were always relaxed. There are two phases for the subsequent constant pressure MD simulation stage: the equilibrium and sampling phases. For both phases, the desired temperature was set to 298.15 K. The pressure was controlled at 1atm with the relaxation time of 2 ps. The temperature was regulated by Langevin dynamics.[63, 64] To constrain all hydrogen atoms, the SHAKE algorithm[33] was applied. After the 20-ns equilibration phase, MD snapshots were collected every 250 ps for at least 160 ns.

4.2.3 MM-PBSA-WSAS binding free energy calculation

One of the most commonly used endpoint methods in free energy calculations is MM-PBSA.[31-33, 65-67] MD simulation is usually applied to capture the dynamics of the system and a set of conformations were collected for post-analyses, including the generation of representative conformation for demonstration, and the MM-PBSA-WSAS binding free energy calculations.[68] In MM-PBSA calculation, the binding free energy ($\Delta G_{MM\text{-}PBSA\text{-}WSAS}$) between a receptor and a ligand to form a complex is expressed in the following equation.

$$\Delta G_{MM-PBSA-WSAS} = \Delta H - T\Delta S = \Delta E_{vdw} + \Delta E_{ele} + \Delta G_p^{sol} + \Delta G_{np}^{sol} - T\Delta S \qquad \textbf{(6)}$$

Where ΔE_{vdw} is the change of MM van der Waals energy, ΔE_{ele} is the change of MM electrostatic energy, ΔG_p^{sol} is the polar solvation free energy, ΔG_{np}^{sol} is the nonpolar solvation free energy. $-T\Delta S$ is the change of conformational entropy, where T is the absolute temperature and ΔS is the change of entropy. It is noted that in **Eq. 6**, the contribution of internal bonded MM energy was cancelled out when using the "Single Trajectory" protocol.[32] In this study, around 660 snapshots were evenly selected for the binding free energy calculations. The Poisson Boltzmann calculation for the polar contribution of the solvation free energy was conducted by using Delphi 98 software.[65] The nonpolar contribution was estimated using solvent-accessible surface areas (SASA) with a surface tension coefficient of 0.00542 kcal/(mol·Å^2) and an offset value of 0.92 kcal/mol. For the estimation of entropic term, we used the weighted solvent accessible surface area (WSAS) method as described elsewhere.[69]

5. Supporting Information

The input parameters for OXY and DZP as well as their metabolites in PBPK models were listed in **Table S1**. The docking scores and calculated K_i for oxycodone and diazepam when binding to CYP3A4 were listed in **Table S2**. **Figure S1** shows the structures of the PBPK model and ADAM model. **Figure S2** shows the docking poses of OXY and DZP in CYP3A4. **Figure S3** shows the 2D and 3D structures of all ligands binding to opioid receptors. **Figure S4** displays the variation of AUC ratio of OXY with a different dosage of DZP when K_i value is ranged from 0.165 to 16.5 μM.

6. Abbreviations

Abbreviation	Full name

DDI	drug-drug interaction
OXY	oxycodone
NOC	noroxycodone
OM	oxymorphone
DZP	diazepam
PK	pharmacokinetic
PD	pharmacodynamic
PBPK	Physiologically-based Pharmacokinetic model
MD	molecular dynamics
MM-PBSA	molecular mechanics/Poisson Boltzmann surface area
MOR	μ-opioid receptor
KOR	κ-opioid receptor
ED	emergency department
FDA	Food and Drug Administration
EMA	European Medicines Agency
BBB	blood-brain-barrier
SD	standard deviations
IV	intravenous
PO	oral
CT	Concentration ~ Time
AUC	area under the curve
AUC_{24h}	the drug exposure from time zero to 24 hours
C_{max}	maximal concentration
T_{max}	time of maximal concentration observed
K_i	inhibitory constant
K_{app}	half-maximal inactivation rate
K_{inact}	inactivation rate of the enzyme
RMSD	root-mean-square deviation
S	substrate

ES	enzyme-substrate complex
E	enzyme
P	product
k_f	forward reaction rate constant
k_r	reverse reaction constant
K_{cat}	K_{cat} is the rate constant of the irreversible reaction of generating product P from ES
K_{eq}	equilibrium constant for the reversible reaction
k_{inact}	inactivation rate of enzyme
K_{obs}	observed inactivation rate constants
ADME	absorption, distribution, metabolism and excretion
ADAM	Advanced Dissolution, Absorption and Metabolism
GI	gastrointestinal
POPC	1-palmitoyl-2-oleoyl-sn-glycero-3-phosphocholine
GAFF	General Amber force field
RESP	restrained electrostatic potential

7. Author Contribution

XQX and JW initialized and designed the research project. BJ, YX and SHL performed simulations and conducted data analysis. All authors contributed to scientific discussions, data interpretations, and manuscript preparation.

8. Competing Interests

There are no competing interests to declare.

9. Acknowledgements

The project described was supported by the National Institutes of Health through Grant ULITR001857. We are grateful to acknowledge the research support from NIH (R01GM79383 to

JW; P30 DA035778-01A1 to XQX) and NSF (1955260 to JW). The authors also thank the computing resources provided by the Center for Research Computing (CRC) at the University of Pittsburgh.

10. References

1. Warner, M.; Trinidad, J. P.; Bastian, B. A.; Miniño, A. M.; Hedegaard, H. Drugs most frequently involved in drug overdose deaths: United States, *Natl. Vital. Stat. Rep.* 2010–2014. **2016**.
2. Olkkola, K.; Ahonen, J., Midazolam and other benzodiazepines. In *Modern Anesthetics*, Springer: 2008; pp 335-360.
3. Jones, C. M.; McAninch, J. K. J. A. j. o. p. m. Emergency department visits and overdose deaths from combined use of opioids and benzodiazepines. *Am. J. Prev. Med.* **2015,** *49*, 493-501.
4. Lee, S. C.; Klein-Schwartz, W.; Doyon, S.; Welsh, C. J. D.; dependence, a. Comparison of toxicity associated with nonmedical use of benzodiazepines with buprenorphine or methadone. *Drug Alcohol Depend.* **2014,** *138*, 118-123.
5. Riley, J.; Eisenberg, E.; Müller-Schwefe, G.; Drewes, A. M.; Arendt-Nielsen, L. Oxycodone: a review of its use in the management of pain. *Curr. Med. Res. Opin.* **2008,** *24*, 175-192.
6. Ordonez Gallego, A.; Gonzalez Baron, M.; Espinosa Arranz, E. Oxycodone: a pharmacological and clinical review. *Clin. Transl. Oncol.* **2007,** *9*, 298-307.
7. Pöyhiä, R.; Vainio, A.; Kalso, E. A review of oxycodone's clinical pharmacokinetics and pharmacodynamics. *J. Pain Symptom Manage.* **1993,** *8*, 63-67.
8. Lalovic, B.; Phillips, B.; Risler, L. L.; Howald, W.; Shen, D. D. Quantitative contribution of CYP2D6 and CYP3A to oxycodone metabolism in human liver and intestinal microsomes. *Drug Metab. Dispos.* **2004,** *32*, 447.
9. Romand, S.; Spaggiari, D.; Marsousi, N.; Samer, C.; Desmeules, J.; Daali, Y.; Rudaz, S. Characterization of oxycodone in vitro metabolism by human cytochromes P450 and UDP-glucuronosyltransferases. *J. Pharm. Biomed. Anal.* **2017,** *144*, 129-137.
10. Calcaterra, N. E.; Barrow, J. C. Classics in Chemical Neuroscience: Diazepam (Valium). *ACS Chem. Neurosci.* **2014,** *5*, 253-260.

11. Lai, S. H.; Yao, Y. J.; Lo, D. S. T. A survey of buprenorphine related deaths in Singapore. *Forensic Sci. Int.* **2006,** *162*, 80-86.
12. Jung, F.; Richardson, T. H.; Raucy, J. L.; Johnson, E. F. Diazepam Metabolism by DNA-Expressed Human 2C P450. *Drug Metab. Dispos.* **1997,** *25*, 133.
13. Goodman, L. S. L. S., Gilman, Alfred, Brunton, Laurence L. Lazo, John S. Parker, Keith L. Goodman & Gilman's the pharmacological basis of therapeutics, 11th. McGraw-Hill Medical Pub; 2006.
14. Greenblatt, D. J.; Divoll, M. Diazepam versus lorazepam: relationship of drug distribution to duration of clinical action. *Adv. Neurol.* **1983,** *34*, 487-491.
15. Nishiya, Y.; Nakamura, K.; Okudaira, N.; Abe, K.; Kobayashi, N.; Okazaki, O. Effects of organic solvents on the time-dependent inhibition of CYP3A4 by diazepam. *Xenobiotica* **2010,** *40*, 1-8.
16. Iribarne, C.; Dréano, Y.; Bardou, L. G.; Ménez, J. F.; Berthou, F. Interaction of methadone with substrates of human hepatic cytochrome P450 3A4. *Toxicology* **1997,** *117*, 13-23.
17. Ji, B.; Liu, S.; Xue, Y.; He, X.; Man, V. H.; Xie, X.-Q.; Wang, J. Prediction of Drug–Drug Interactions Between Opioids and Overdosed Benzodiazepines Using Physiologically Based Pharmacokinetic (PBPK) Modeling and Simulation. *Drugs in R&D* **2019,** *19*, 297-305.
18. Jones, J. D.; Mogali, S.; Comer, S. D. Polydrug abuse: A review of opioid and benzodiazepine combination use. *Drug Alcohol Depend.* **2012,** *125*, 8-18.
19. Stitzer, M. L.; Griffiths, R. R.; McLellan, A. T.; Grabowski, J.; Hawthorne, J. W. Diazepam use among methadone maintenance patients: Patterns and dosages. *Drug Alcohol Depend.* **1981,** *8*, 189-199.
20. Marzolini, C.; Rajoli, R.; Battegay, M.; Elzi, L.; Back, D.; Siccardi, M. Physiologically Based Pharmacokinetic Modeling to Predict Drug-Drug Interactions with Efavirenz Involving Simultaneous Inducing and Inhibitory Effects on Cytochromes. *Clin. Pharmacokinet.* **2017,** *56*, 409-420.
21. Budha, N. R.; Ji, T.; Musib, L.; Eppler, S.; Dresser, M.; Chen, Y.; Jin, J. Y. Evaluation of Cytochrome P450 3A4-Mediated Drug-Drug Interaction Potential for Cobimetinib

Using Physiologically Based Pharmacokinetic Modeling and Simulation. *Clin. Pharmacokinet.* **2016,** *55*, 1435-1445.

22. Tang, J.; Amin Usmani, K.; Hodgson, E.; Rose, R. L. In vitro metabolism of fipronil by human and rat cytochrome P450 and its interactions with testosterone and diazepam. *Chem. Biol. Interact.* **2004,** *147*, 319-329.
23. Wolf, B. C.; Lavezzi, W. A.; Sullivan, L. M.; Flannagan, L. M. One hundred seventy two deaths involving the use of oxycodone in Palm Beach County. *J. Forensic Sci.* **2005,** *50*, 192-195.
24. Greenblatt, D. J.; Woo, E.; Allen, M. D.; Orsulak, P. J.; Shader, R. I. Rapid Recovery From Massive Diazepam Overdose. *JAMA* **1978,** *240*, 1872-1874.
25. Divoll, M.; Greenblatt, D. J.; Lacasse, Y.; Shader, R. I. Benzodiazepine overdosage: plasma concentrations and clinical outcome. *Psychopharmacology (Berl)* **1981,** *73*, 381-383.
26. Cox, R. F.; Collins, M. A. The effects of benzodiazepines on human opioid receptor binding and function. *Anesth. Analg.* **2001,** *93*, 354-358 , 353rd contents page.
27. Smith, M. T.; Edwards, S. R.; Nielsen, C. K. Oxycodone's mechanism of action and potency differences after spinal and systemic routes of administration. *Anesthesiology* **2007,** *106*, 1063-1064; author reply 1064-1065.
28. Lalovic, B.; Kharasch, E.; Hoffer, C.; Risler, L.; Liu-Chen, L. Y.; Shen, D. D. Pharmacokinetics and pharmacodynamics of oral oxycodone in healthy human subjects: role of circulating active metabolites. *Clin. Pharmacol. Ther.* **2006,** *79*, 461-479.
29. Thompson, C. M.; Wojno, H.; Greiner, E.; May, E. L.; Rice, K. C.; Selley, D. E. Activation of G-proteins by morphine and codeine congeners: insights to the relevance of O- and N-demethylated metabolites at mu- and delta-opioid receptors. *J. Pharmacol. Exp. Ther.* **2004,** *308*, 547-554.
30. Massova, I.; Kollman, P. A. Combined molecular mechanical and continuum solvent approach (MM-PBSA/GBSA) to predict ligand binding. *Perspectives in Drug Discovery and Design* **2000,** *18*, 113-135.
31. Kuhn, B.; Gerber, P.; Schulz-Gasch, T.; Stahl, M. Validation and Use of the MM-PBSA Approach for Drug Discovery. *J. Med. Chem.* **2005,** *48*, 4040-4048.

32. Junmei, W.; Tingjun, H.; Xiaojie, X. Recent Advances in Free Energy Calculations with a Combination of Molecular Mechanics and Continuum Models. *Curr. Comput. Aided Drug Des.* **2006,** *2*, 287-306.
33. Hou, T.; Wang, J.; Li, Y.; Wang, W. Assessing the performance of the MM/PBSA and MM/GBSA methods. 1. The accuracy of binding free energy calculations based on molecular dynamics simulations. *J. Chem. Inf. Model.* **2011,** *51*, 69-82.
34. Weng, G.; Wang, E.; Chen, F.; Sun, H.; Wang, Z.; Hou, T. Assessing the performance of the MM/PBSA and MM/GBSA methods. 9. Prediction reliability of binding affinities and binding poses for protein-peptide complexes. *Phys. Chem. Chem. Phys.* **2019,** *21*.
35. Wang, L.; Wu, Y.; Deng, Y.; Kim, B.; Pierce, L.; Krilov, G.; Lupyan, D.; Robinson, S.; Dahlgren, M. K.; Greenwood, J., et al. Accurate and Reliable Prediction of Relative Ligand Binding Potency in Prospective Drug Discovery by Way of a Modern Free-Energy Calculation Protocol and Force Field. *J. Am. Chem. Soc.* **2015,** *137*, 2695-2703.
36. He, X.; Liu, S.; Lee, T.-S.; Ji, B.; Man, V. H.; York, D. M.; Wang, J. Fast, Accurate, and Reliable Protocols for Routine Calculations of Protein–Ligand Binding Affinities in Drug Design Projects Using AMBER GPU-TI with ff14SB/GAFF. *ACS Omega* **2020,** *5*, 4611-4619.
37. Krippendorff, B. F.; Neuhaus, R.; Lienau, P.; Reichel, A.; Huisinga, W. Mechanism-based inhibition: deriving K(I) and k(inact) directly from time-dependent IC(50) values. *J. Biomol. Screen.* **2009,** *14*, 913-923.
38. Friesner, R. A.; Banks, J. L.; Murphy, R. B.; Halgren, T. A.; Klicic, J. J.; Mainz, D. T.; Repasky, M. P.; Knoll, E. H.; Shelley, M.; Perry, J. K., et al. Glide: a new approach for rapid, accurate docking and scoring. 1. Method and assessment of docking accuracy. *J. Med. Chem.* **2004,** *47*, 1739-1749.
39. Jamei, M.; Bajot, F.; Neuhoff, S.; Barter, Z.; Yang, J.; Rostami-Hodjegan, A.; Rowland-Yeo, K., A Mechanistic Framework for In Vitro–In Vivo Extrapolation of Liver Membrane Transporters: Prediction of Drug–Drug Interaction Between Rosuvastatin and Cyclosporine. *Clin. Pharmacokinetic.* 2013; Vol. 53.
40. Kostewicz, E. S.; Aarons, L.; Bergstrand, M.; Bolger, M. B.; Galetin, A.; Hatley, O.; Jamei, M.; Lloyd, R.; Pepin, X.; Rostami-Hodjegan, A., et al. PBPK models for the

prediction of in vivo performance of oral dosage forms. *Eur. J. Pharm. Sci.* **2014,** *57*, 300-321.

41. Moore, C.; Kelley-Baker, T.; Lacey, J. Interpretation of oxycodone concentrations in oral fluid. *J. Opioid Manag.* **2012,** *8*, 161-166.
42. Jones, A. W.; Larsson, H. Distribution of diazepam and nordiazepam between plasma and whole blood and the influence of hematocrit. *Ther. Drug Monit.* **2004,** *26*, 380-385.
43. Seaton, S.; Reeves, M.; McLean, S. Oxycodone as a component of multimodal analgesia for lactating mothers after Caesarean section: Relationships between maternal plasma, breast milk and neonatal plasma levels. *Aust. N. Z. J. Obstet. Gynaecol.* **2007,** *47*, 181-185.
44. Mandelli, M.; Tognoni, G.; Garattini, S. Clinical Pharmacokinetics of Diazepam. *Clin. Pharmacokinet.* **1978,** *3*, 72-91.
45. Chin, P. K. L.; Jensen, B. P.; Larsen, H. S.; Begg, E. J. Adult age and ex vivo protein binding of lorazepam, oxazepam and temazepam in healthy subjects. *Br. J. Clin. pharmacol.* **011,** *72*, 985-989.
46. Li, Y.; Sun, D.; Palmisano, M.; Zhou, S. Slow drug delivery decreased total body clearance and altered bioavailability of immediate- and controlled-release oxycodone formulations. *Pharmacol. Res. Perspect.* **2016,** *4*, e00210.
47. Marsousi, N.; Daali, Y.; Rudaz, S.; Almond, L.; Humphries, H.; Desmeules, J.; Samer, C. F. Prediction of Metabolic Interactions With Oxycodone via CYP2D6 and CYP3A Inhibition Using a Physiologically Based Pharmacokinetic Model. *CPT: Pharmacometrics Syst. Pharmacol.* **2014,** *3*, e152-e152.
48. Divoll, M.; Greenblatt, D. J.; Harmatz, J. S.; Shader, R. I. Effect of age and gender on disposition of temazepam. *J. Pharm. Sci.* **1981,** *70*, 1104-1107.
49. Kenworthy, K. E.; Clarke, S. E.; Andrews, J.; Houston, J. B. Multisite Kinetic Models for CYP3A4: Simultaneous Activation and Inhibition of Diazepam and Testosterone Metabolism. *Drug Metab. Dispos.* **2001,** *29*, 1644.
50. Shou, M.; Mei, Q.; Ettore, M. W., Jr.; Dai, R.; Baillie, T. A.; Rushmore, T. H. Sigmoidal kinetic model for two co-operative substrate-binding sites in a cytochrome P450 3A4 active site: an example of the metabolism of diazepam and its derivatives. *Biochem. J.* **1999,** *340 (Pt 3)*, 845-853.

51. Zhou, S.; Yung Chan, S.; Cher Goh, B.; Chan, E.; Duan, W.; Huang, M.; McLeod, H. L. Mechanism-based inhibition of cytochrome P450 3A4 by therapeutic drugs. *Clin. Pharmacokinet.* **2005,** *44*, 279-304.

52. Kanamitsu, S. I.; Ito, K.; Okuda, H.; Ogura, K.; Watabe, T.; Muro, K.; Sugiyama, Y. Prediction of in vivo drug-drug interactions based on mechanism-based inhibition from in vitro data: inhibition of 5-fluorouracil metabolism by (E)-5-(2-Bromovinyl)uracil. *Drug Metab. Dispos.* **2000,** *28*, 467-474.

53. Jo, S.; Kim, T.; Iyer, V. G.; Im, W. CHARMM-GUI: a web-based graphical user interface for CHARMM. *J. Comput. Chem.* **2008,** *29*, 1859-1865.

54. Jorgensen, W. L.; Chandrasekhar, J.; Madura, J. D.; Impey, R. W.; Klein, M. L. Comparison of simple potential functions for simulating liquid water. *J. Chem. Phys.* **1983,** *79*, 926-935.

55. Maier, J. A.; Martinez, C.; Kasavajhala, K.; Wickstrom, L.; Hauser, K. E.; Simmerling, C. ff14SB: Improving the Accuracy of Protein Side Chain and Backbone Parameters from ff99SB. *J. Chem. Theory Comput.* **2015,** *11*, 3696-3713.

56. Wang, J.; Wolf, R. M.; Caldwell, J. W.; Kollman, P. A.; Case, D. A. Development and testing of a general amber force field. *J. Comput. Chem.* **2004,** *25*, 1157-1174.

57. Bayly, C. I.; Cieplak, P.; Cornell, W.; Kollman, P. A. A well-behaved electrostatic potential based method using charge restraints for deriving atomic charges: the RESP model. *J. Phys. Chem.* **1993,** *97*, 10269-10280.

58. Frisch, M. J.; Trucks, G. W.; Schlegel, H. B.; Scuseria, G. E.; Robb, M. A.; Cheeseman, J. R.; Scalmani, G.; Barone, V.; Petersson, G. A.; Nakatsuji, H., et al. *Gaussian 16 Rev. B.01*, Wallingford, CT, 2016.

59. Wang, J.; Wang, W.; Kollman, P. A.; Case, D. A. Automatic atom type and bond type perception in molecular mechanical calculations. *J. Mol. Graph. Model* **2006,** *25*, 247-260.

60. Case, D. A., Betz RM, Cerutti DS et al AMBER 2016. *University of California, San Francisco* **2016**.

61. Gotz, A. W.; Williamson, M. J.; Xu, D.; Poole, D.; Le Grand, S.; Walker, R. C. Routine Microsecond Molecular Dynamics Simulations with AMBER on GPUs. 1. Generalized Born. *J. Chem. Theory Comput.* **2012,** *8*, 1542-1555.

62. Salomon-Ferrer, R.; Gotz, A. W.; Poole, D.; Le Grand, S.; Walker, R. C. Routine Microsecond Molecular Dynamics Simulations with AMBER on GPUs. 2. Explicit Solvent Particle Mesh Ewald. *J. Chem. Theory Comput.* **2013,** *9*, 3878-3888.
63. Izaguirre, J. A.; Catarello, D. P.; Wozniak, J. M.; Skeel, R. D. Langevin stabilization of molecular dynamics. *J. Chem. Phys.* **2001,** *114*, 2090-2098.
64. Ryckaert, J.-P.; Ciccotti, G.; Berendsen, H. J. C. Numerical integration of the cartesian equations of motion of a system with constraints: molecular dynamics of n-alkanes. *J. Chem. Inf. Model.* **1977,** *23*, 327-341.
65. Rocchia, W.; Alexov, E.; Honig, B. Extending the Applicability of the Nonlinear Poisson−Boltzmann Equation: Multiple Dielectric Constants and Multivalent Ions. *J. Phys. Chem. B* **2001,** *105*, 6754-6754.
66. Swanson, J. M.; Henchman, R. H.; McCammon, J. A. Revisiting free energy calculations: a theoretical connection to MM/PBSA and direct calculation of the association free energy. *Biophys. J.* **2004,** *86*, 67-74.
67. Wang, E.; Sun, H.; Wang, J.; Wang, Z.; Liu, H.; Zhang, J. Z. H.; Hou, T. End-Point Binding Free Energy Calculation with MM/PBSA and MM/GBSA: Strategies and Applications in Drug Design. *Chem. Rev.* **2019,** *119*, 9478-9508.
68. Xu, L.; Sun, H.; Li, Y.; Wang, J.; Hou, T. Assessing the Performance of MM/PBSA and MM/GBSA Methods. 3. The Impact of Force Fields and Ligand Charge Models. *J. Phys. Chem. B* **2013,** *117*, 8408-8421.
69. Wang, J.; Hou, T. Develop and Test a Solvent Accessible Surface Area-Based Model in Conformational Entropy Calculations. *J Chem. Inf. Model.* **2012,** *52*, 1199-1212.
70. Friedman, H.; Greenblatt, D. J.; Peters, G. R.; Metzler, C. M.; Charlton, M. D.; Harmatz, J. S.; Antal, E. J.; Sanborn, E. C.; Francom, S. F. Pharmacokinetics and pharmacodynamics of oral diazepam: effect of dose, plasma concentration, and time. *Clin. Pharmacol. Ther.* **1992,** *52*, 139-150.
71. Klotz, U.; Avant, G. R.; Hoyumpa, A.; Schenker, S.; Wilkinson, G. R. The effects of age and liver disease on the disposition and elimination of diazepam in adult man. *J. Clin. Investig.* **1975,** *55*, 347-359.

Tables

Table 1. The AUC, C_{max} and T_{max} of 30 mg PO OXY, 10 mg PO DZP and 1 mg/kg DZP. SD is standard deviation and all units are shown in parenthesis. a: Observed 1 and Observed 2 are the experimental data collected from Drugs.com (https://www.drugs.com). b, c: Observed data for PO and IV DZP are respectively obtained from two reports.[70, 71]

Dosing Strategy		AUC (SD) (ng·h/mL)	C_{max} (SD) (ng/mL)	T_{max} (SD) (h)
OXY PO 30 mg (0-24 h)	Observed 1[a]	268.2 (60.7)	39.3 (14.0)	2.6 (3)
	Observed 2[a]	277.0 (89.6)	48.5 (15.9)	1.5 (NA)
	Predicted	311.83 (150.67)	38.0 (14.69)	1.2 (0.31)
DZP PO 10 mg (0-12 h)	Observed[b]	1530 (464.33)	317 (89.55)	1.32 (0.56)
	Predicted	1677.12 (434.66)	221.89 (51.5)	1.15 (0.35)
DZP IV 0.1 mg/kg (0-24 h)	Observed[c]	2198.5 (NA)	NA	NA
	Predicted	1932.46 (582.83)	NA	NA

Table 2. The AUC ratio and C_{max} ratio of the DDI profiles for PO OXY and 10 mg, 100 mg and 500 mg and 1000 mg of PO/IV DZP. CI is the 95% Confidence Interval. AUC_{24h} ratio is the exposure of AUC ratio from the time 0 to 24 hours.

Dosing Strategy	Formulation	AUC_{24h} ratio	CI [5%,95%]	C_{max} ratio	CI [5%,95%]
OXY 30 mg + DZP 10mg	PO	1.01	[1.00,1.01]	1.01	[1.00,1.01]
	IV	1.00	[1.00,1.01]	1.00	[1.00,1.00]
OXY 30 mg + DZP 100mg	PO	1.05	[1.03,1.07]	1.04	[1.02,1.06]
	IV	1.03	[1.02,1.05]	1.02	[1.01,1.04]
OXY 30 mg + DZP 500mg	PO	1.13	[1.09,1.19]	1.09	[1.06,1.14]
	IV	1.12	[1.07,1.17]	1.07	[1.04,1.12]
OXY 30 mg + DZP 1000mg	PO	1.20	[1.12,1.29]	1.12	[1.07,1.19]
	IV	1.18	[1.18,1.27]	1.10	[1.05,1.17]

Table 3. The AUC ratio and C_{max} ratio of the DDI profiles for PO OXY and 10 mg, 100 mg, 500 mg and 1000 mg of PO DZP when applying mixed-type inhibition to the DDI model. CI is the 95% Confidence Interval. AUC_{24h} ratio is the exposure of AUC ratio from the time 0 to 24 hours.

Dosing Strategy	AUC_{24h} ratio	CI [5%,95%]	C_{max} ratio	CI [5%,95%]
OXY 30 mg + DZP 10mg	1.01	[1.01,1.02]	1.01	[1.00,1.02]
OXY 30 mg + DZP 100mg	1.07	[1.04,1.09]	1.04	[1.03,1.06]
OXY 30 mg + DZP 500mg	1.21	[1.13,1.31]	1.10	[1.06,1.16]
OXY 30 mg + DZP 1000mg	1.30	[1.17,1.48]	1.13	[1.07,1.22]

Table 4. The docking results (kcal/mol) for opioids and diazepam targeting to both the active and inactive X-ray structures of MOR and KOR.

	OXY	DZP	4VO	BF0	CVV	JDC
active MOR	-6.38	-6.81	-9.47	-6.07	-	-
inactive MOR	-5.93	-6.38	-5.42	-7.39	-	-
active KOR	-7.20	-6.51	-	-	-7.47	-7.32
inactive KOR	-5.49	-5.50	-	-	-6.42	-8.68

Table 5. Calculated binding free energies (kcal/mol) and the individual energy terms for opioids and DZP using the MM-PBSA-WSAS method.

Ligands	ΔE_{vdw}	ΔE_{ele}	ΔG_p^{sol}	ΔG_{np}^{sol}	$T\Delta S$	$\Delta G_{MM-PBSA}$
	active MOR					
4VO	-50.45±0.08	-5.75±0.01	35.59±0.11	-4.41±0.01	-22.05±0.04	-2.98±0.13
BF0	-53.48±0.11	-14.88±0.37	53.08±0.45	-4.91±0.01	-23.34±0.02	3.15±0.18
OXY	-36.05±0.06	-4.43±0.49	22.52±0.55	-2.86±0.00	-19.62±0.02	-1.19±0.11
DZP	-33.51±0.06	-8.64±0.19	24.81±0.23	-2.88±0.00	-18.89±0.07	-1.33±0.05
	inactive MOR					
4VO	-41.34±0.03	-5.54±0.09	29.17±0.25	-3.81±0.00	-19.55±0.01	-1.97±0.21
BF0	-45.60±0.16	-27.56±0.36	52.26±0.26	-4.00±0.01	-21.83±0.04	-3.06±0.28
OXY	-40.95±0.10	-15.44±0.07	33.55±0.10	-2.97±0.00	-20.41±0.02	-5.40±0.05
DZP	-39.33±0.16	-8.78±0.08	32.32±0.31	-2.84±0.00	-19.69±0.02	1.07±0.13
	active KOR					
CVV	-65.93±0.14	-20.98±0.21	58.27±0.07	-4.90±0.00	-26.76±0.01	-6.78±0.24
JDC	-59.00±0.21	-24.28±0.43	59.69±0.47	-5.51±0.00	-25.64±0.02	-3.46±0.22
OXY	-38.56±0.06	-9.43±0.16	30.69±0.25	-2.96±0.00	-19.92±0.04	-0.34±0.16
DZP	-36.84±0.12	0.18±0.14	18.49±0.06	-2.90±0.01	-19.30±0.03	-1.78±0.19
	inactive KOR					
CVV	-57.17±0.03	-22.40±0.21	61.26±0.31	-4.90±0.00	-24.88±0.04	1.66±0.46
JDC	-59.08±0.15	-29.80±0.22	67.32±0.48	-5.32±0.00	-26.63±0.03	-0.25±0.28
OXY	-38.73±0.08	-9.25±0.13	28.95±0.15	-2.95±0.00	-19.97±0.03	-2.01±0.29
DZP	-37.97±0.13	-15.50±0.09	39.58±0.12	-2.73±0.01	-20.12±0.04	3.49±0.09

For Table of Contents Use Only

Drug-Drug Interaction Between Oxycodone and Diazepam by a Combined *in silico* Pharmacokinetic and Pharmacodynamic Modeling Approach

Beihong Ji[1, 2,+], Ying Xue[1, 2,+], Yuanyuan Xu[1, 2], Shuhan Liu[1, 2], Albert H Gough[3], Xiang-Qun Xie[1, 2,*], Junmei Wang[1, 2,*]

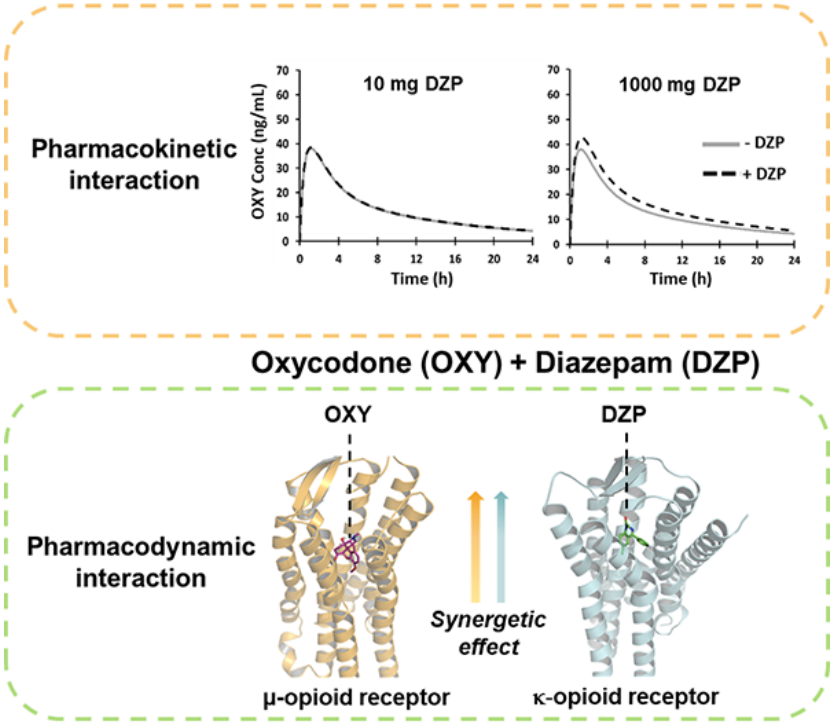

2.0 × 1.75 inches with 300 dpi resolution